Scientia Iranica B (2017) 24(2), 727–739

Sharif University of Technology
Scientia Iranica
Transactions B: Mechanical Engineering
www.scientiairanica.com

Research Note

Stress analyses in single-deck and double-deck floating roofs subjected to earthquake ground motions

F.G. Golzar[a], R. Shabani[a,*] and S. Tariverdilo[b]

a. *Department of Mechanical Engineering, Faculty of Engineering, Urmia University, Urmia, Iran.*
b. *Department of Civil Engineering, Faculty of Engineering, Urmia University, Urmia, Iran.*

Received 29 June 2014; received in revised form 25 November 2015; accepted 18 July 2016

KEYWORDS
Cylindrical tank;
Sloshing response;
Earthquake;
Floating roof.

Abstract. This paper investigates the stress patterns in circular single- and double-deck floating roofs excited by earthquake ground motions. Variational formulation is employed to derive the governing equations. Response of the floating roofs to different classes of ground motions including near-field and far-field records is evaluated. Results indicate that far-field earthquakes produce larger wave elevation but smaller bending stresses in the floating roof. Moreover, the bending stresses in double-deck roofs emerge in a smooth and approximately symmetric pattern with a peak around the mid-span radius while the peak values of bending stress in single-deck floating roofs occur at the vicinity of deck center and at the deck-pontoon interface. The results can have practical implications in the design process of floating-roof cylindrical tanks.

1. Introduction

Floating roofed storage tanks are employed to store different liquids in petroleum and petrochemical industries. Floating roofs eliminate evaporation by covering the exposed liquid surface and thus reduce the material loss and air pollution. In addition, they reduce the possibility of fire hazard in highly flammable hydrocarbon vapors due to sources like earthquakes, static electricity, cigarette smoking, etc. [1]. Taking into account the past major earthquakes, it has been found that the liquid sloshing could destroy the floating roofs [2]. For instance, during the 2003 Tokachi-Oki earthquake, seven oil storage tanks of floating roof type located at Tomakomi, Hokkaido, Japan were seriously damaged. Damages included the sinking of the floating roofs, which led one of the seven tanks to a whole surface fire. Therefore, the inclusion of fluid-structure coupling in design and analysis of floating roofs subjected to ground motions is important.

Employing variational principle, Sakai et al. [3] calculated the natural frequencies of floating roofs. Isshiki and Nagata [4] derived the governing equations of a floating plate by assuming Hamilton's principle for plate and Kelvin's principle for water. Amabili and Kwak [5] utilized Hankel transformation to analyze the vibrational properties of circular plates with different forms of uniform boundary conditions. Investigations were continued by Matsui, who employed Fourier-Bessel series to derive the governing equations of motion for a base excited storage tank with double-deck [6] and single-deck [7] floating roofs. Matsui [6,7] investigated the impact of different flexural modes on the response metrics including roof deflection, liquid pressure imposed on the tank wall, and bending stresses within the roof. In a shaking table test, Nagaya et al. [8] investigated the vibrational characteristics of roofs and showed the strong dependency of damping

*. *Corresponding author.*
E-mail address: r.shabani@urmia.ac.ir (R. Shabani)

ratio on roof type. Epstein [9] utilized shooting method and showed the effect of structural parameters on the stresses in single-deck floating roofs. Added mass factors have been used to explore the effect of fluid on natural frequencies of axisymmetric circular plates with different boundary conditions [10]. Sun et al. [11] carried out a finite element method in a single-deck floating roof subjected to water loading. Shabani et al. [12] used a variational approach to evaluate the equilibrium conditions between the elastic and buoyant forces and depicted the contribution of membrane and flexural constituents to the overall roof stiffness. Using extended Hamilton's principle, Golzar et al. [13] introduced a set of results predicting behavior of tanks with double-deck roofs when excited by different types of earthquakes. Shabani and Golzar [14] extracted the governing nonlinear equation of a floating roof of a seismically excited cylindrical tank. They showed the suppressing effect of nonlinearities on the sloshing heights for a wide range of tank dimensions. In an experimental study, De Angelis et al. [15] studied the response of base isolated cylindrical tanks with and without roofs to earthquake excitations. They showed that the base isolators and floating roofs could reduce the wall pressure and oscillation amplitudes significantly. Later, Shabani [16] investigated the induced stresses in single-deck floating roofs on seismic storage tanks. He depicted two critical locations in the deck roofs: one near the center of the roof and the other along the deck-pontoon interface. He concluded that the near-source ground motions produce larger stresses at the inner critical radius of the deck, but far-field ground motions lead to larger stresses in deck-pontoon interface.

In some references [6,13], the double-deck roofs have been investigated and in other reports [7,16], the stress patterns in single-deck roofs are reported. However, the present paper compares the stress pattern of the single- and double-deck floating roofs and discusses the changes in this pattern due to change in the deck type. Applying the Hamilton's variational principle to the floating roof and contained liquid, simultaneously, the responses of roofed storage tanks to different earthquakes, including near-source and far-field records, are investigated. Direct numerical integration method is employed to calculate the deflection of roof and corresponding stresses. Stress patterns produced in double-deck roofs are found and compared with the single-deck roof results qualitatively and quantitatively. Moreover, the effect of earthquake type is studied for a practical range of tank dimensions. The results may prove useful in design considerations.

2. Mathematical model

Figure 1 illustrates a cylindrical tank of radius, R,

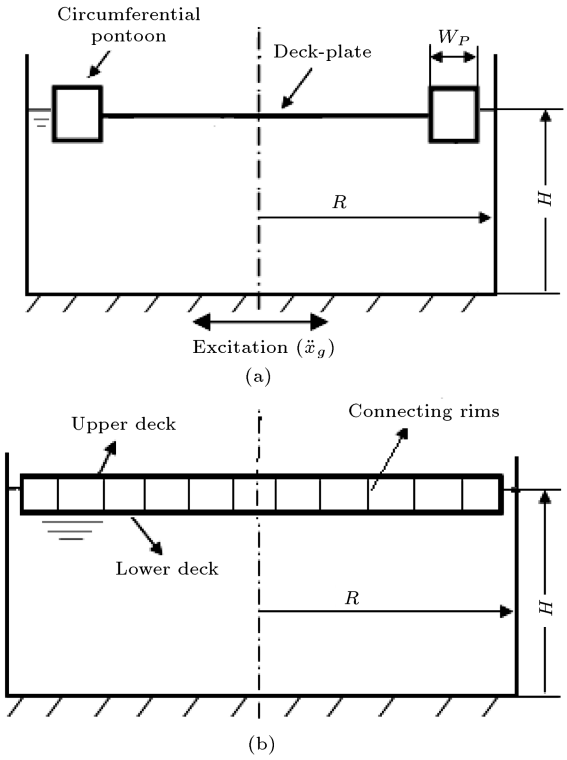

Figure 1. Cylindrical liquid storage tank with (a) single-deck and (b) double-deck floating roofs.

filled to a height, H, with an incompressible liquid of density, ρ, and equipped with an elastic floating roof. The conventional floating roofs can be categorized into two types: single-deck and double-deck. Single-deck roofs (Figure 1(a)) are composed of a circumferential buoyant ring (pontoon) with relatively large stiffness surrounding an inner circular plate (deck) with small thickness and stiffness. Double-deck roofs (Figure 1(b)), on the other hand, consist of upper and lower decks connected by structural rims. For changing fluid level in the tank, the floating roof should stay in contact with contained fluid. Therefore, there is a relatively large gap between the side wall and the floating roof edge. On the other hand, to protect vapor escape through floating roof perimeter, special seals are employed, where single- and double-wiper seals and liquid-mounted foam seals are the most common types. These seals could also operate as damping element to prevent the floating roofs from side wall impacts. In this study, effect of the lateral side wall forces on the floating roofs is ignored as this study only considers vertical vibration of the floating deck due to fluid sloshing. In the mathematical modeling, the following assumptions have been made:

1. The tank has a rigid flat bottom and a rigid cylindrical wall;
2. The tank is excited by the unidirectional ground excitation, $\ddot{x}_g$;

3. The contained liquid is an inviscid and incompressible fluid in an irrotational motion;
4. The floating roofs deform in bending only;
5. The floating roofs are always in contact with the contained liquid;
6. Effect of the lateral side wall forces on the floating roofs is ignored;
7. The proposed model does not account for vertical component of the seismic excitation.

Laplacian equation, together with the impermeability and kinematic boundary conditions, may be used to fully define the movement of the liquid inside the enclosed tank volume:

$$\nabla^2\Phi = 0, \quad 0\le r\le R, \quad 0\le\theta<2\pi, \quad 0\le z\le H, \tag{1}$$

$$\frac{\partial\Phi}{\partial z} = 0, \quad z = 0, \tag{2}$$

$$\frac{\partial\Phi}{\partial r} = \dot{x}_g\cos\theta \qquad r = R. \tag{3}$$

Imposing these conditions, the velocity potential is obtained in the following form:

$$\Phi(r,z,\theta) = r\dot{x}_g\cos\theta + \Phi_0,$$

$$\Phi_0 = \sum_{k=1}^{\infty} A_k \frac{J_1\left(\frac{\varepsilon_k r}{R}\right)}{J_1(\varepsilon_k)} \frac{\cosh\left(\frac{\varepsilon_k z}{R}\right)}{\cosh\left(\frac{\varepsilon_k H}{R}\right)}\cos\theta,$$

$$k = 1, 2, 3, \ldots \tag{4}$$

where A_k is the kth unknown time-dependent shape factors and ε_k is the kth eigenvalue of the velocity potential obtained from the characteristic equation $J_1'(\varepsilon_k) = 0$. Lateral vibration of the floating roof can be considered as a weighted summation of free vibration mode shapes of a free-edge circular plate:

$$\eta(r,\theta,t) = \sum_{i=1}^{\infty} B_i(t) X_i(r)\cos\theta, \tag{5}$$

where B_i denotes the generalized coordinates and X_i denotes the radial mode shapes consisting of rigid and elastic modes [17]:

$$X_1(r) = \frac{r}{R},$$

$$X_i(r) = \left[\alpha_i J_1\left(\kappa_i\frac{r}{R}\right) + \beta_i I_1\left(\kappa_i\frac{r}{R}\right)\right],$$

$$i = 2, 3, \cdots \tag{6}$$

κ_i represents the radial eigenvalues of the free-edge circular plate. J_1 denotes the Bessel function of the first kind of order one and I_1 denotes the modified Bessel function of the first kind of order one. Bearing in mind that the roof and liquid stay in complete contact, the assembled Lagrangian of the coupled system, accounting for the kinetic and potential energies, is written in form of the sum of the roof Lagrangian L_R and liquid Lagrangian L_l [18] as shown in Box I. Making use of the Hamiltonian principle, the equation of motion of roof is obtained in the following matrix form (see Appendix A):

$$M_R[P]\left\{\ddot{B}\right\} + (D_R[Q] + \rho_L g[U])\{B\} + \rho_L[T]\left\{\dot{A}\right\} + \rho_L\ddot{x}_g\{F\} = 0, \tag{8}$$

$$\left[T^t\right]\left\{\dot{B}\right\} - [S]\{A\} = 0. \tag{9}$$

Elements of matrices P, Q, U, F, S and T are specified as follows:

$$L = L_R + L_l = \int_{r=0}^{R}\int_{\theta=0}^{2\pi}\left\{\frac{1}{2}M_R\dot{\eta}^2 - \frac{1}{2}D_R\left[\begin{array}{l}\left(\frac{\partial^2\eta}{\partial r^2}\right)^2 + \left(\frac{1}{r}\frac{\partial\eta}{\partial r} + \frac{1}{r^2}\frac{\partial^2\eta}{\partial\theta^2}\right)^2 \\ +2\nu\left(\frac{\partial^2\eta}{\partial r^2}\right)\left(\frac{1}{r}\frac{\partial\eta}{\partial r} + \frac{1}{r^2}\frac{\partial^2\eta}{\partial\theta^2}\right) \\ +2(\upsilon-1)\left(\frac{1}{r}\frac{\partial^2\eta}{\partial r\partial\theta} - \frac{1}{r^2}\frac{\partial\eta}{\partial\theta}\right)\end{array}\right]\right\} r dr d\theta$$

$$+ \int_{r=0}^{R}\int_{\theta=0}^{2\pi}\rho_L\left[-\frac{1}{2}\left(\frac{\partial\Phi_0}{\partial z}\right)\Phi_0 + \frac{\partial\eta}{\partial t}\Phi - \frac{1}{2}g\eta^2\right] r dr d\theta, \tag{7}$$

where M_R and D_R denote the mass and rigidity of the roof.

Box I

Table 1. Seismic data used in this study [13].

Input ground motion	Kobe (1995)	Imperial valley (1940)	Tokachi-oki (2003)	Tohoku (2011)
Duration (s)	40	40	290	300
PGA (g)	0.4862	0.3130	0.0800	0.1397
Epicentral distance (km)	8.7	13	227	364

$$P_{ij} = \int_0^R X_i X_j r dr,$$

$$Q_{ij} = \int_0^R X_i'' X_j'' r dr + \int_0^R \left(\frac{1}{r}X_i' - \frac{1}{r^2}X_i\right)\left(\frac{1}{r}X_j' - \frac{1}{r^2}X_j\right)(3-2\nu) r dr + \int_0^R \left[X_i''\left(\frac{1}{r}X_j' - \frac{1}{r^2}X_j\right) + X_j''\left(\frac{1}{r}X_i' - \frac{1}{r^2}X_i\right)\right]\nu r dr,$$

$$U_{ij} = \int_0^R X_i X_j r dr,$$

$$T_{ij} = \int_{r=0}^R X_i \frac{J_1(\varepsilon_j r/R)}{J_1(\varepsilon_j)} r dr,$$

$$F_i = \int_{r=0}^R r X_i r dr,$$

$$S_{jj} = \frac{R}{2}\varepsilon_j \tanh\left(\frac{\varepsilon_j H}{R}\right)\left(1 - \frac{1}{\varepsilon_j^2}\right). \quad (10)$$

Combining Eqs. (8) and (9) yields the following equation [13]:

$$\left(M_R[P] + \rho_L[T]\left[S^{-1}\right]\left[T^t\right]\right)\left\{\ddot{B}\right\} + \left(D_R[Q] + \rho_L g[U]\right)\{B\} + \rho_L \ddot{x}_g\{F\} = 0. \quad (11)$$

This equation suggests that both dynamic and static couplings exist between the roof and oscillating fluid, resulting in a coupled set of equations. The mass matrix in Eq. (11) is composed of two parts: $M_R[P]$ accounting for the presence of floating plate and $\rho_L[t][S^{-1}][T^t]$ representing the added inertial effect of the liquid. Likewise, stiffness matrix is composed of $D_R[Q]$ accounting for the plate stiffness and $\rho_L g[U]$ representing the added stiffness due to fluid co-vibration.

By truncating Eqs. (4) and (5) to limited numbers n and m, respectively, the obtained set of equations may be solved to yield the generalized coordinates and, consequently, plate deflection and liquid velocity potential. Moreover, radial and circumferential bending moments resulting in the bending stresses in roof cross-section are calculated by the following formulae [13]:

$$M_r = -D_R\left(\frac{\partial^2\eta}{\partial r^2} + \nu\left[\frac{1}{r}\frac{\partial\eta}{\partial r} + \frac{1}{r^2}\frac{\partial^2\eta}{\partial\theta^2}\right]\right), \quad (12)$$

$$M_\theta = -D_R\left(\left[\frac{1}{r}\frac{\partial\eta}{\partial r} + \frac{1}{r^2}\frac{\partial^2\eta}{\partial\theta^2}\right] + \nu\frac{\partial^2\eta}{\partial r^2}\right). \quad (13)$$

3. Excitation characteristics

To study the dynamic response of a seismically excited roofed tank, the following earthquakes data were used as base excitations [13]: 090 components of 1995 Kobe earthquake at Japan recorded at Nishi-Akashi station (KOBE/NIS000), 180 components of 1940 Imperial Valley earthquake recorded at El Centro station (IMPVALL/I-ELC180), EW component of 2003 Tokachi-oki earthquake recorded at Tomakomai station (HKD1290309260450EW), and EW component of 2011 Tohoku earthquake (Eastern Japan earthquake) recorded at Chiba station (CHB0091103111446). Table 1 shows the duration, peak ground acceleration, and epicentral distance of earthquake records. Time histories and Fourier decomposition of the records are shown in Figures 2 and 3, respectively.

Kobe and Imperial Valley earthquakes have similar frequency contents with spectral peaks at low periods and are classified as near-source earthquakes. However, Tokachi-oki and Tohoku with broad band frequency content are classified as long-period, far-field records. Near-source earthquakes act in a shorter time interval, but impose larger accelerations to the structures compared to long-period, far-field earthquakes.

4. Simulation results

In this section, recordings of the aforementioned earthquake ground motions are used as base excitation input

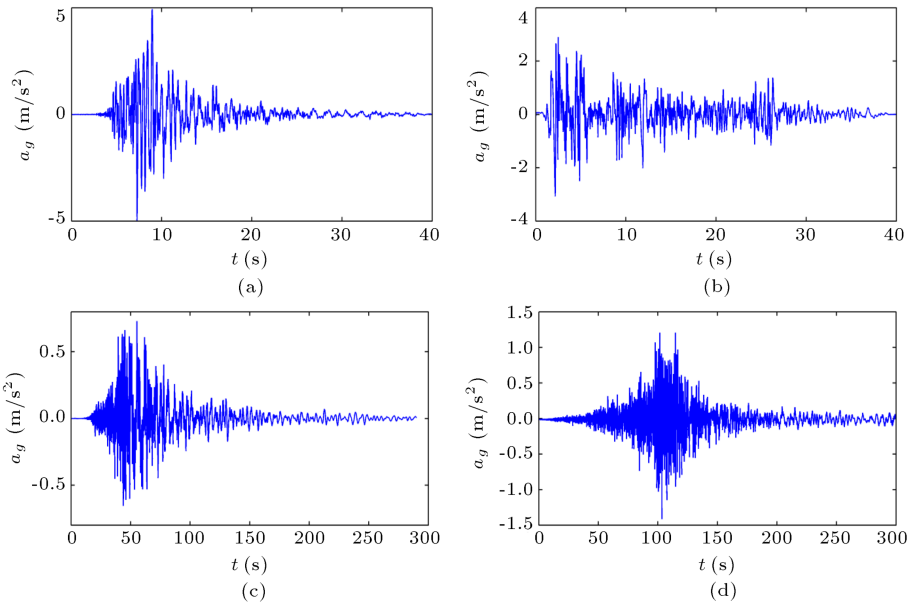

Figure 2. Time histories of ground motions [13]: (a) Kobe, (b) Imperial Valley, (c) Tokachi-oki, and (d) Tohoku.

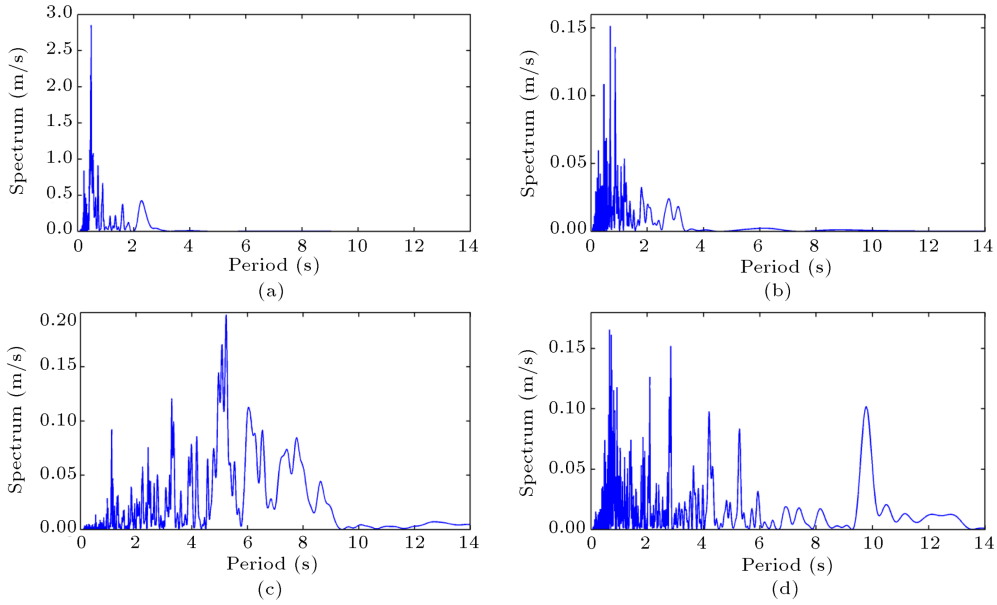

Figure 3. Fast Fourier Transform (FFT) of ground motions [13]: (a) Kobe, (b) Imperial Valley, (c) Tokachi-oki, and (d) Tohoku.

for a wide range of tank dimensions. It should be mentioned that in actual structures, some form of damping will emerge, owing to sources such as viscous liquid-wall interaction or/and friction between roof and wall. To account for the energy dissipation in the system, damping matrix C is added to Eq. (11):

$$\left(M_R[P]+\rho_L[T]\left[S^{-1}\right]\left[T^t\right]\right)\left\{\ddot{B}\right\}+[C]\left\{\dot{B}\right\} + \left(D_R[Q]+\rho_L g[U]\right)\{B\}+\rho_L x_g\{F\}=0. \quad (14)$$

The stiffness proportional damping is utilized with the modal damping ratio depicted in Table 2. The selected value (0.005) is in accordance with the experimental findings of Nagaya et al. [8], where it was also stated that the stiffness proportional damping was appropriate for double-deck roofs. In numerical simulations, Newmark's method is employed to solve the governing equation [13].

4.1. Numerical results for double-deck floating roof

In this section, recordings of the aforementioned earthquakes are used as base excitation for a wide range of tank dimensions with the geometrical and material properties shown in Table 2.

Table 2. Geometrical and material properties of the tank with a double-deck floating roof.

Contained liquid height, H	15 m
Roof areal mass density, M_R	120 kg/m^2
Roof bending rigidity, D_R	1.612×10^5 kN.m
Roof thickness, h_R	800 mm
Liquid density, ρ_L	800 kg/m^3
Damping ratio, double-deck, ζ	0.01
Effective cross sectional coefficient, A_{eff}	1050 mm^2
Poisson's ratio, ν	0.3
Number of modes adopted for liquid sloshing, m	33
Number of modes adopted for roof vibration, n	5

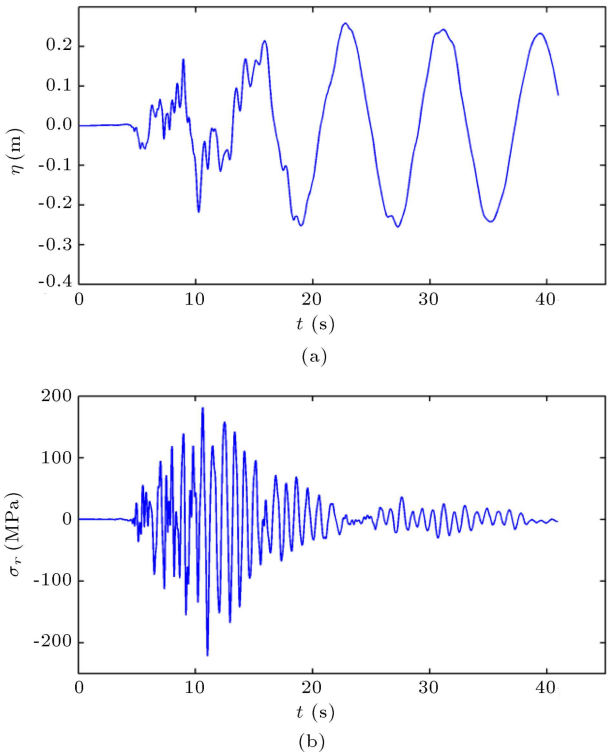

Figure 4. Time history of double-deck roof due to near-field Kobe excitation: (a) Roof edge deflection, and (b) induced radial stress.

Response of double-deck floating roof to the near-field excitation of Kobe is shown in Figure 4. Similar behavior is witnessed when the Imperial Valley excitation is used (it is not shown here). Maximum radial stress in the roof occurs during the major earthquake period (Figure 4(b)) while the roof oscillation continues till the end of the excitation (Figure 4(a)).

Time histories of roof deflection and radial stress in a tank subjected to far-field excitations of Tokachi-oki and Tohoku earthquakes are shown in Figure 5(a), (b), (c), and (d), respectively. Response of the tank subjected to Tokachi-oki shows that both metrics reach their peak values simultaneously with the input excitation and gradually fade, oscillating in the fundamental mode of the coupled system (Figure 5(a) and (b)). It is shown that the roof deflection is larger; nevertheless, smaller stresses are witnessed in the roof cross section. Figure 5(c) and (d) show the response of a tank subjected to Tohoku earthquake. Due to the record's rich frequency content in low and high periods, floating roof behavior in this case shows similarities with both near-source records of Kobe and Imperial Valley and far-field, long period record of Tokachi-oki. It is observed that the radial stress decreases swiftly after the major earthquake duration has passed while roof maintains its high-amplitude oscillation till the end of the record, like the phenomenon seen in near-source excitations.

Peak values of stresses are slightly higher than those of the Tokachi-oki excitation, which are attributed to the greater share of the second mode in the oscillation. In conclusion, the vibration of roof-edge is dominated by the fundamental period of the system [13] while the oscillation of bending stresses is well affected by the frequency content of the excitation record. The richer the content of the excitation at lower periods, the higher the contribution of higher modes.

Quantitative difference between the results of near-source and far-field excitations is highlighted in Figure 6, where the peak value diagrams in the previous figures are shown altogether. It is observed that vertical roof deflection is far larger in the case of far-field excitations as a direct result of rich frequency content around fundamental period (Figure 3). On the other hand, near-source earthquakes impose larger bending stresses as the participation of second natural mode in the stresses is much greater due to their rich content at lower periods (Figure 3).

Figure 7 compares the peak values of deflection and stresses for tanks with different radii, which could be considered as response spectra of these parameters. Note that in evaluating these results, all the properties are kept intact except for the radius of the tank and roof. Stronger response spectrum of far-field earthquakes renders the produced roof deflection larger and more radius-dependent than the case of near-field earthquakes, where the absolute value of deflection is approximately invariant for all tank radii. On the contrary, bending stresses caused by near-source excitations are considerably larger in the majority of radius span as a consequence of stronger frequency content at lower periods, which gives rise to the second-mode

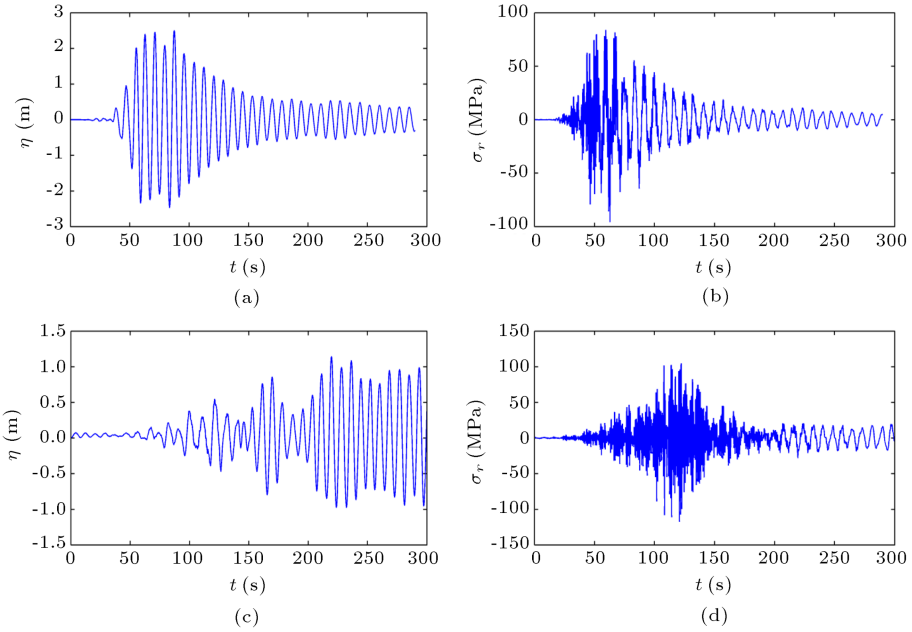

Figure 5. Time history of roof edge deflection and radial stress due to far-field excitations: (a) and (b) Tokachi-oki, (c) and (d) Tohoku.

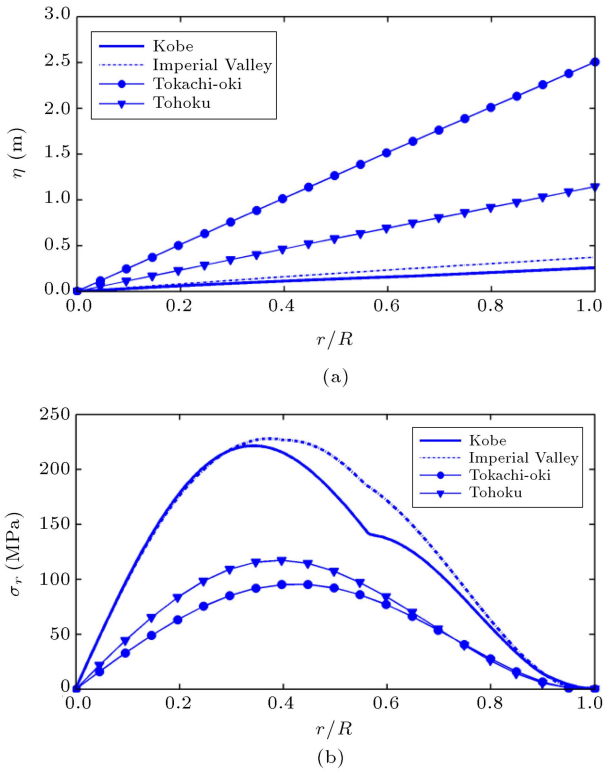

Figure 6. Comparison of effects of earthquakes on a specific tank ($H = 15$, $R = 25$): (a) Roof deflection and (b) radial bending stress.

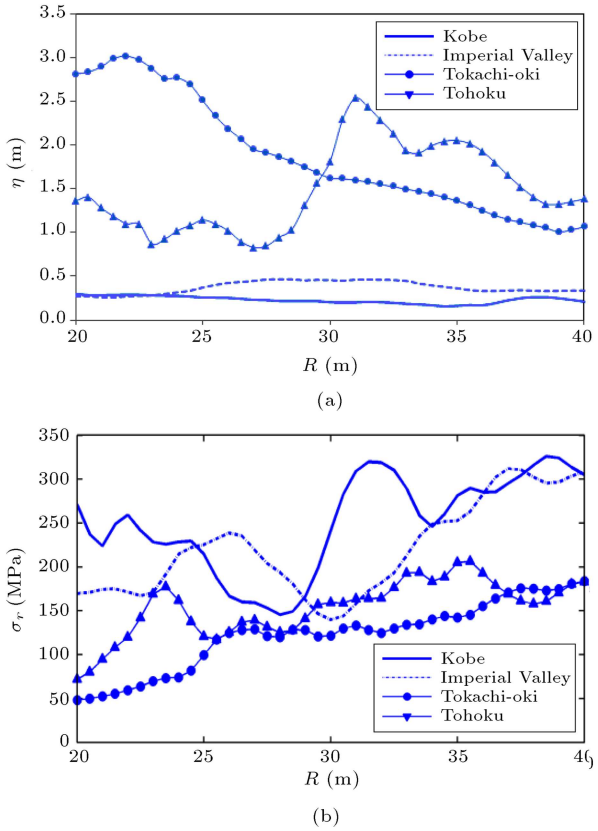

Figure 7. Effect of earthquakes on tanks with different dimensions: (a) Roof deflection and (b) radial bending stress.

contribution in the stresses. As it was observed, the second mode of oscillation had a crucial contribution to the bending stresses. This makes the absolute value of stress highly radius-dependent since any small change in the radius may result in the overlapping of periods with frequency peaks of excitation inputs, thus boosting the bending stress. It is concluded that in

designing the floating roofed cylindrical tanks, far-field earthquakes should be considered for determining the free-board while the bending strength of the roof should be set great enough to endure near-source earthquakes.

4.2. Numerical results for single-deck floating roof

This section is devoted to the numerical analysis of single-deck floating roofs subjected to the 4 seismic records described in the previous sections. Table 3 shows the numerical data used in the calculations.

4.2.1. Note on radial mode shapes

Radial mode shapes of the single-deck roof differ from those of the double-deck due to its radius-dependent bending characteristics. The mode shapes of the double-deck are those of a circular plate with uniform geometrical and material properties while in the single-deck roof, deck plate and pontoon possess different characteristics rendering their flexural behavior considerably different. Deck plate behaves as an elastic plate, but the relatively large bending stiffness of the pontoon prevents it from undergoing radius-dependent elastic deformation. Thus, the behavior of deck in the radial direction, relative to the pontoon, is analogous to the behavior of a cantilever to its fixed end. This makes the interface radius susceptible to high bending stresses and, potentially, a failure point. To extract the mode shapes, Eq. (6) has to be modified to account for the zero curvature of the pontoon, and zero relative deflection and slope in the deck-pontoon interface. Second- and third-mode shapes are illustrated in Figure 8 for the sake of comparison.

Response of the single-deck storage tank to near-source excitation of Kobe is depicted in Figure 9. The edge-deflection of the floating roof is similar to that of the double-deck type in terms of amplitude (Figure 9(a)).

Dynamic behavior of single-deck roof subjected to

Table 3. Geometrical and material properties of the tank with a single-deck floating roof.

Tank height, H	15 m
Tank radius, R	25 m
Pontoon width, W_P	3 m
Deck areal mass density, M_d	58 kg/m^2
Pontoon areal mass density, M_P	173 kg/m^2
Pontoon bending rigidity, D_P	2.7×10^5 kN.m
Deck plate thickness, h_D	4.5 mm
Liquid density, ρ	800 kg/m^3
Damping ratio, ζ	0.005
Poisson's ratio, ν	0.3
Adopted modes for roof vibration, n	29
Adopted modes for liquid sloshing, m	33

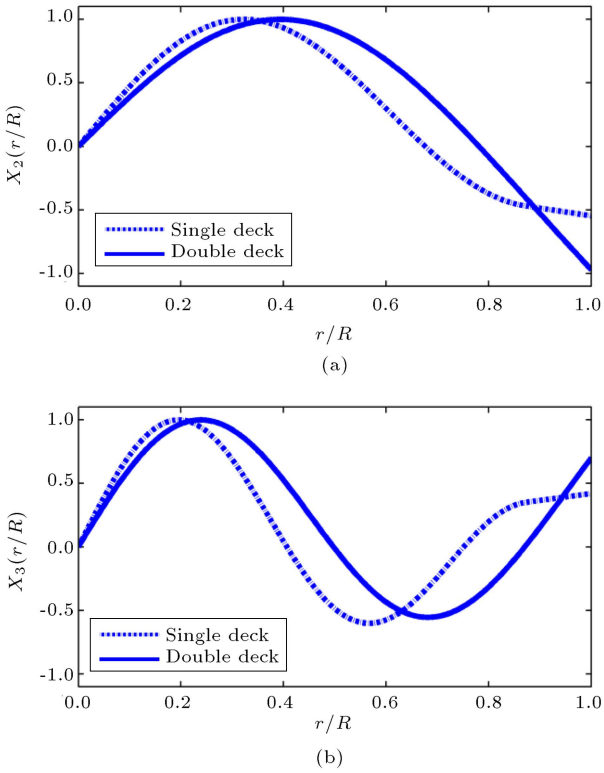

Figure 8. Comparison of radial mode shapes for single-deck and double-deck roofs: (a) 2nd mode and (b) 3rd mode.

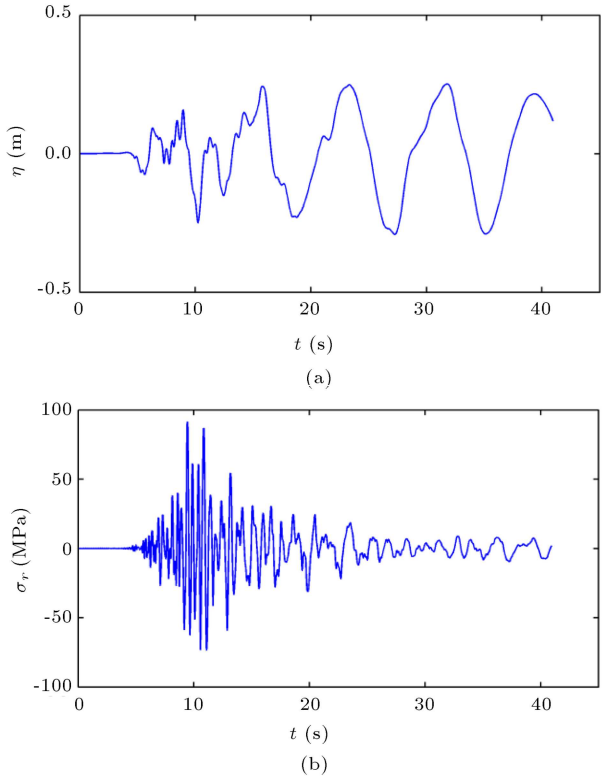

Figure 9. Time history of single-deck roof due to near-field Kobe excitation: (a) Roof edge deflection and (b) radial stress.

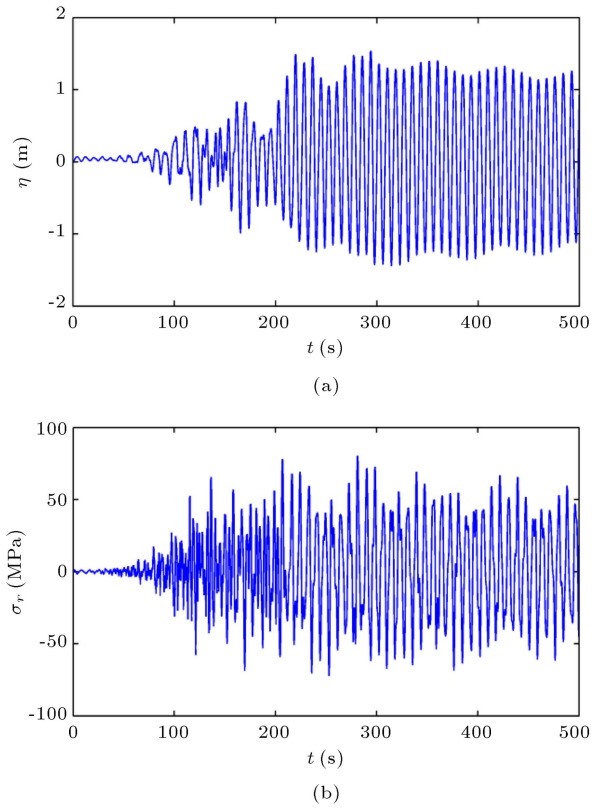

Figure 10. Time history of single-deck roof due to far-field excitation of Tohoku: (a) Roof edge deflection, and (b) radial stress.

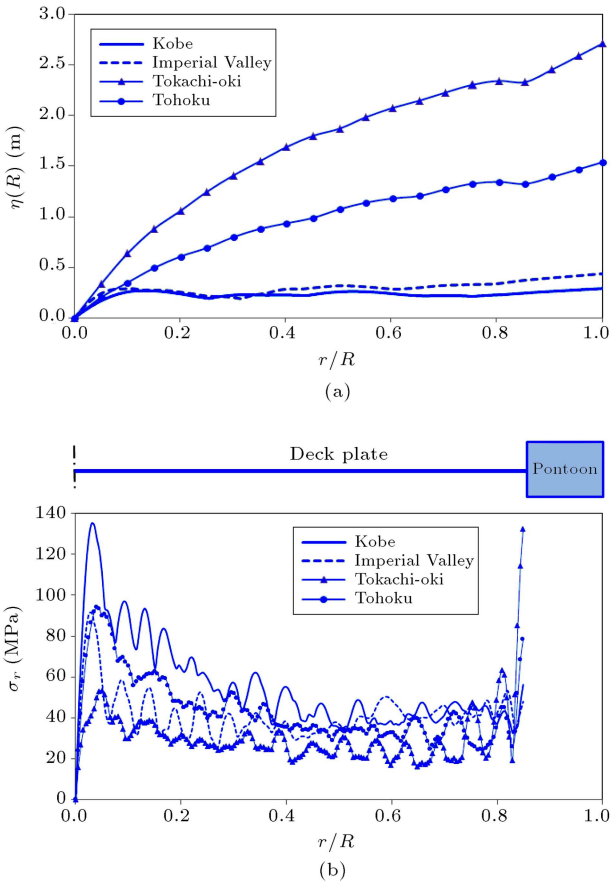

Figure 11. Comparison of effects of earthquakes on the responses of single-deck floating roof: (a) Roof deflection, and (b) raidal bending stress.

Far-Field excitation of Tohoku is shown in Figure 10. Similar behavior is witnessed when the Tokachi-oki excitation is used (it is not shown here). Despite the near-source excitations, here, the amplitude of bending stress shows a low rate of dissipation (Figure 10(b)). Roof shows high-amplitude oscillatory motion till the end of the earthquake (Figure 10(a)), producing considerable bending stresses in the roof cross section. Stresses induced within the roof share characteristics of both near-source excitations of Kobe and Imperial Valley and far-field Tokachi-oki as the Tohoku earthquake possesses rich frequency content at both high and low periods.

For the sake of comparison, vertical deflection and radial stresses in the deck plate, caused by the mentioned 4 ground motions, are plotted altogether in Figure 11. Similar to the tanks with double-deck roof, far-field long-period earthquakes produce larger roof deflections compared to near-source earthquakes. Stresses in the pontoon were assumed zero and, thus, are not plotted here. Again, it is seen that near-source ground motions of Kobe and Imperial Valley produce large stresses in the central critical radius while far-field long-period earthquakes of Tokahci-oki and Tohoku result in large stresses along the deck-pontoon interface. Moreover, Tohoku earthquake imposes considerably large stresses at the central critical radius as its frequency content is rich at low periods as well as high periods, activating higher modes of vertical deflection of the deck plate.

Figure 12 compares the peak values of stresses within the single-deck floating roof with different radii, which could be considered as response spectra of stresses. The radius of the roof and tank is swept from 20 to 40 meters to include the typical range of tanks used in the petroleum industries. Radial stresses at the two most vulnerable radii are plotted with respect to the radius of the tank. Strong content of the near-source earthquakes of Kobe and Imperial Valley results in the higher modes of the coupled system being activated and, thus, the stresses at the central critical radius, which are significantly influenced by the higher modes and take larger values compared to the case of far-field excitations. The contrary is valid for the stresses occurring along the deck-pontoon interface; the oscillation of these stresses is majorly controlled by the fundamental period of the system, i.e., far-field earthquakes, which possess strong content at high periods and render greater values at this radius. The stresses along the deck-pontoon interface show an overall de-

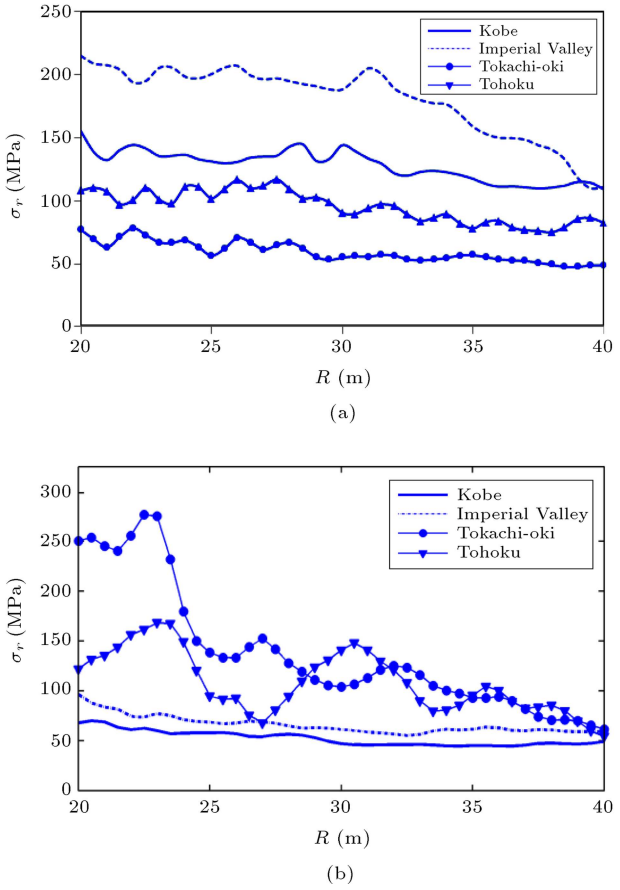

Figure 12. Effect of earthquakes on tanks with different dimensions: (a) Radial stress at central critical radius and (b) radial stress at deck-pontoon interface.

scending trend with respect to radius. Consequently, for sufficiently wide tanks, deck-pontoon interface is no longer a high-risk critical point compared to the central critical radius. In conclusion, the design criteria for the strength of the deck plate may be divided into two parts; strength at the central radii, which should be determined by the characteristics of near-source ground motions; and bending strength along its connection with annular pontoon, which should be predicted by the probable hazards of far-field quakes.

4.3. Comparison of stress patterns in single-deck and double-deck roofs

Dissimilarities in stress patterns occurring in single-deck and double-deck floating roofs are presented in Figure 13. In case of near-source ground motions, double-deck roofs experience more destructive stresses compared to single-deck roofs and the most vulnerable points are located at $r \approx 0.35R$. On the other hand, when the tank is subjected to far-field long-period ground motions, the values of bending stress in double-deck roofs are of the same scale as those of single-deck roofs. It could be stated that design criteria for the double-deck roofs are controlled by the requirements of near-source quakes; but, deck strength in single-deck roofs has to be determined by accounting for both near-source and far-field seismic hazards.

5. Conclusion

This paper studied the stress analyses in floating

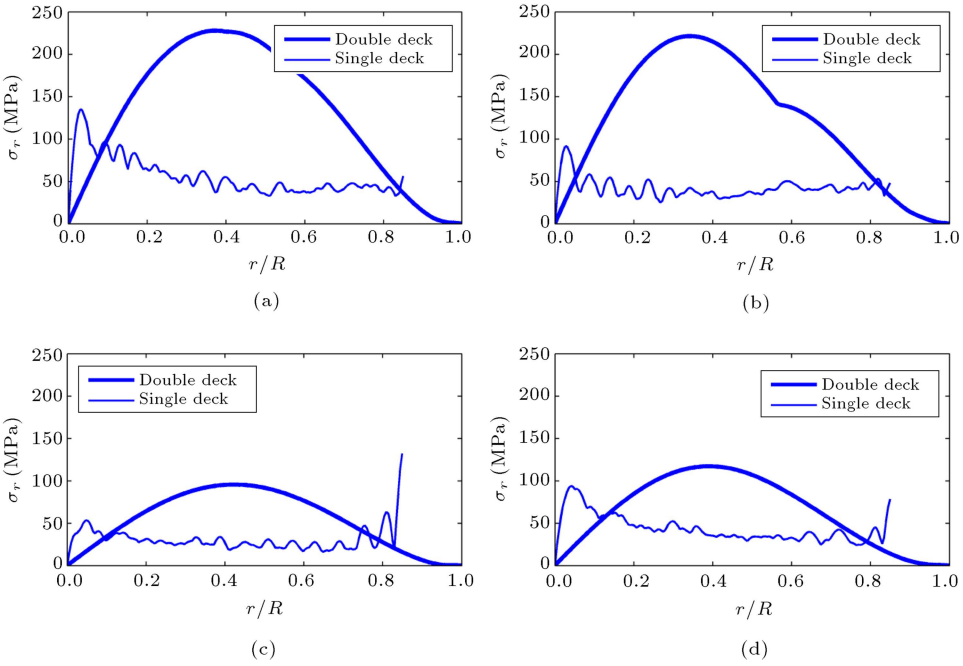

Figure 13. Stress patterns in single-deck and double-deck roofs: (a) Kobe, (b) Imperial Valley, (c) Tokachi-oki, and (d) Tohoku.

roofs subjected to near-source and long-period far-field ground motion records. Two types of floating roofs, single-deck and double-deck, were utilized in the simulations. It was revealed that higher modes have significant impact on the stresses, especially at central parts of single-deck roof. Near-source excitations proved more destructive in case of double-deck roofs, while single-deck roofs were prone to failure when excited by far-field ground motions as well as near-source ones. Results suggest that near-source ground motions produce larger stresses in the case of double-deck roofs and also at the inner critical radius of single-deck roofs, but far-field ground motions lead to larger stresses in deck-pontoon interface. It is concluded that free-board design should be carried out taking into account long-period earthquakes while bending stress evaluation requires consideration of both near-source and far-field hazards.

References

1. Changa, J.I. and Linb, C-C. "A study of storage tank accidents", *Journal of Loss Protection in the Process Industries*, **19**(1), pp. 51-59 (2006).
2. Hatayama, K., Zama, S., Nishi, H., Yamada, M., Hirokawa, M. and Inoue, R. "The damages of oil storage tanks during the 2003 Tokachi-oki earthquake and the long period ground motions", *Proceedings of the JSCE-AIJ Joint Symposium on Huge Subduction Earthquakes-Wide Area Strong Ground Motion Prediction*, pp. 7-18 (2005).
3. Sakai, F., Nishimura, M. and Ogawa, H. "Sloshing behavior of floating-roof oil storage tanks", *Comput. Struct.*, **19**(1-2), pp. 183-192 (1984).
4. Isshiki, H. and Nagata, S. "Variational principles related to motions of an elastic plate floating on a water surface", *Proceeding of the 11th International Offshore and Polar Engineering Conference*, Stavanger, Norway, pp. 190-197 (2001).
5. Amabili, M. and Kwak, M.K. "Free vibration of circular plates coupled with liquids: revising the lamb problem", *J. Fluids Struct.*, **10**(7), pp. 743-761 (1996).
6. Matsui, T. "Sloshing in a cylindrical liquid storage tank with a floating roof under seismic excitation", *ASME J. Pressure Vessel Technol.*, **129**(4), pp. 557-566 (2007).
7. Matsui, T. "Sloshing in a cylindrical liquid storage tank with a single deck type floating roof under seismic excitation", *ASME J. Pressure Vessel Technol.*, **131**(2), pp. 557-566 (2009).
8. Nagaya, T., Matsui, T. and Wakasa, T. "Model tests on sloshing of a floating roof in a cylindrical liquid storage tank under seismic excitation", *Proceedings of the ASME Pressure Vessels and Piping Division Conference*, San Antonio, Texas, Illinois, USA, PVP2008-61675 (2008).
9. Epstein, H.I. "Stress and displacements for floating pan roofs", *Comput. Struct.*, **15**(4), pp. 433-438 (1982).
10. Kwak, M.K. and Kim, K.C. "Axisymmetric vibration of circular plates in contact with fluid", *J. Sound Vib.*, **146**(3), pp. 381-389 (1991).
11. Sun, X., Liu, Y., Wang, J., Cen, Z. "Stress and deflection analyses of floating roofs based on a load-modifying method", *Int. J. Press. Vessels Pip.*, **85**, pp. 728-738 (2008).
12. Shabani, R., Tariverdilo, S., Salarie, H. and Rezazadeh, G. "Importance of flexural and membrane stiffnesses in large deflection analysis of floating roofs", *Appl. Math. Modell.*, **34**, pp. 2426-2436 (2010).
13. Golzar, F.G., Shabani, R., Tariverdilo, H. and Rezazadeh, G. "Sloshing response of floating roofed liquid storage tanks subjected to earthquakes of different types", *ASME J. Pressure Vessel Technol.*, **134**(5), 051801-13 (2012).
14. Shabani, R. and Golzar, F.G. "Large deflection analysis of floating roofs subjected to earthquake ground motions", *Nonlinear Anal. Real World Appl.*, **13**, pp. 2034-2048 (2012).
15. De Angelis, M., Giannini, R. and Paolacci, F. "Experimental investigation on the seismic response of a steel liquid storage tank equipped with floating roof by shaking table tests", *Earthquake Eng. Struct. Dyn.*, **39**, pp. 377-396 (2009).
16. Shabani, R., "Stress patterns in single deck floating roofs subjected to ground motion accelerations", *International Journal of Engineering-Transactions C: Aspects*, **26**(12), pp. 1495-1504 (2013).
17. Thomson, W.T. and Dahleh, M.D., *Theory of Vibration with Applications*, Prentice Hall, Chap. 11 (1998).
18. Meirovitch, L., *Principles and Techniques of Vibrations*, Prentice Hall, Chap. 7 (1997).

Appendix A

Equations of motion

Substituting Eqs. (4) and (5) into Eq. (7), the Lagrangian is calculated by Eq. (A.1) as shown in Box A.1. Referring to the principle of variation, time integral of variation of Lagrangian vanishes in any desired time interval:

$$\int_{t_1}^{t_2} \delta L dt = 0, \tag{A.2}$$

which requires the multiplicands of both unknowns δA

$$L=\Bigg\{\int_{r=0}^{R}\left(\sum_{i=1}^{\infty}\dot{B}_iX_i\right)\left(\sum_{j=1}^{\infty}\dot{B}_jX_j\right)\frac{1}{2}M_Rrdr+\int_{r=0}^{R}\left(\sum_{i=1}^{\infty}B_iX_i''\right)\left(\sum_{j=1}^{\infty}B_j(t)X_j''(r)\right)\left(-\frac{1}{2}D_R\right)rdr$$
$$+\int_{r=0}^{R}\left(\frac{1}{r}\sum_{i=1}^{\infty}B_i(t)X_i'-\frac{1}{r^2}\sum_{i=1}^{\infty}B_iX_i\right)\left(\frac{1}{r}\sum_{j=1}^{\infty}B_jX_j'-\frac{1}{r^2}\sum_{j=1}^{\infty}B_jX_j\right)\left(-\frac{1}{2}D_r\right)rdr$$
$$+\int_{r=0}^{R}\left(\sum_{i=1}^{\infty}B_iX_i''\right)\left(\frac{1}{r}\sum_{j=1}^{\infty}B_jX_j'-\frac{1}{r^2}\sum_{j=1}^{\infty}B_jX_j\right)(-\nu D_R)rdr+\int_{r=0}^{R}\left[\sum_{k=1}^{\infty}\frac{\varepsilon_k}{R}A_k\frac{J_1(\varepsilon_kr/R)}{J_1(\varepsilon_k)}\tanh\left(\varepsilon_k\frac{H}{R}\right)\right]$$
$$\left[\sum_{l=1}^{\infty}A_l\frac{J_1(\varepsilon_lr/R)}{J_1(\varepsilon_l)}\right]\left(-\frac{1}{2}\rho_L\right)rdr+\int_{r=0}^{R}\left[\sum_{i=1}^{\infty}\dot{B}_iX_i\right]\left[r\dot{x}_g+\sum_{k=1}^{\infty}A_k\frac{J_1(\varepsilon_kr/R)}{J_1(\varepsilon_k)}\right]\rho_Lrdr$$
$$+\int_{r=0}^{R}\rho_L\left(-\frac{1}{2}g\right)\left[\sum_{i=1}^{\infty}B_iX_i\right]\left[\sum_{j=1}^{\infty}B_jX_j\right]rdr\Bigg\}\times\int_{\theta=0}^{2\pi}\cos^2\theta d\theta. \tag{A.1}$$

Box A.1

and δB to be zero:

$$\int_{r=0}^{R}\left(\sum_{i=1}^{\infty}\ddot{B}_iX_i\right)X_j(-M_R)rdr$$
$$+\int_{r=0}^{R}\left(\sum_{i=1}^{\infty}B_iX_i''\right)X_j''(-D_R)rdr$$
$$+\int_{r=0}^{R}\left(\frac{1}{r}\sum_{i=1}^{\infty}B_iX_i'-\frac{1}{r^2}\sum_{i=1}^{\infty}B_iX_i\right)\left(\frac{1}{r}X_j'-\frac{1}{r^2}X_j\right)(-D_R)rdr$$
$$+\int_{r=0}^{R}\left[\left(\frac{1}{r}\sum_{i=1}^{\infty}B_iX_i'\right)X_j''+\left(\frac{1}{r}\sum_{i=1}^{\infty}B_iX_i''\right)X_j'-\left(\frac{1}{r^2}\sum_{i=1}^{\infty}B_iX_i\right)X_j''-\left(\frac{1}{r^2}\sum_{i=1}^{\infty}B_iX_i''\right)X_j\right]$$
$$(-\nu D_R)rdr-\int_{r=0}^{R}\left[r\ddot{x}_g+\sum_{k=1}^{\infty}\dot{A}_k\frac{J_1\left(\frac{\varepsilon_kr}{R}\right)}{J_1(\varepsilon_k)}\right]X_j\rho_Lrdr$$
$$+\int_{r=0}^{R}\left(\sum_{i=1}^{\infty}B_iX_i\right)X_j(\rho_Lg)rdr=0, \tag{A.3}$$

$$\int_{r=0}^{R}\left[\frac{\varepsilon_k}{R}\frac{J_1(\varepsilon_kr/R)}{J_1(\varepsilon_k)}\tanh\left(\varepsilon_k\frac{H}{R}\right)\right]$$
$$\left[\sum_{l=1}^{\infty}A_1\frac{J_1(\varepsilon_lr/R)}{J_1(\varepsilon_l)}\right]\left(-\frac{1}{2}\rho_L\right)rdr$$
$$+\int_{r=0}^{R}\left[\sum_{l=1}^{\infty}\frac{\varepsilon_l}{R}A_l\frac{J_1(\varepsilon_lr/R)}{J_1(\varepsilon_l)}\tanh\left(\varepsilon_l\frac{H}{R}\right)\right]$$
$$\left[\frac{J_1(\varepsilon_kr/R)}{J_1(\varepsilon_k)}\right]\left(-\frac{1}{2}\rho_L\right)rdr$$
$$+\int_{r=0}^{R}\left[\sum_{i=1}^{\infty}\dot{B}_iX_i\right]\left[\frac{J_1(\varepsilon_kr/R)}{J_1(\varepsilon_k)}\right]\rho_Lrdr=0. \tag{A.4}$$

These equations are rewritten in the following matrix form:

$$M_R[P]\left\{\ddot{B}\right\}+(D_R[Q]+\rho_Lg[U])\{B\}+\rho_L[T]\left\{\dot{A}\right\}+\rho_L\ddot{x}_g\{F\}=0, \tag{A.5}$$

$$[T^t]\left\{\dot{B}\right\}-[S]\{A\}=0. \tag{A.6}$$

Biographies

Farzin Ghahramanian Golzar received his BS degree in Mechanical Engineering from the University of

Tabriz, Iran and his MS degree in the field of Applied Mechanics from Urmia University, Iran, in 2012. He is now a PhD Candidate in the field of Structural Mechanics in University of Canterbury, New Zealand. His research interests include liquid-coupled vibration, stability in mems structures, and earthquake induced structural vibrations.

Rasoul Shabani received his BS degree in Mechanical Engineering from KNT University of Technology in 1993. He received his MS degree in 1996 and his PhD in 2006 from Sharif University of Technology, Iran. He is now a Professor in the Mechanical Engineering Department at Urmia University. His research interest includes fluid structure interaction, chaotic vibrations and nonlinear dynamics, and control of MEMS.

Saeid Tariverdilo received his BS degree in Civil Engineering in 1994 and his MS and PhD degrees in 1997 and 2001 in Structural Engineering from Sharif University of Technology, Iran. He is now a Professor in the Civil engineering Department at Urmia University. His research interest includes fluid structure interaction.